17th World Conference on Earthquake Engineering, 17WCEE
Sendai, Japan - September 27th to October 2nd, 2021

THE POSSIBLE CORRELATIONS BETWEEN STRONG GROUND MOTIONS OF THE THREE LARGE EARTHQUAKES IN CHINA AND LANDSLIDE DISTRIBUTIONS

Yuzhu. Bai [(1)]
[(1)] *Associate Researcher, Institute of Geology, China Earthquake Administration, e-mail: yuzhubai2008@126.com*

Abstract

In this work, the correlations between spatial distributions of landslide points and strong ground motion parameters of the three strong earthquakes happened recently in China are qualitatively investigated. Three strong events are the Lushan (4-20-2013), Wenchuan (5-12-2008), and Jiuzhaigou (8-8-2017) earthquakes. In order to reconstruct the near filed strong ground motions of these earthquakes, the broadband ground simulation method of Schmedes et al (2010) is applied. After validation of the computation results of the Lushan earthquake against the station record, the reconstructed fields of ground motions including the parameters of the peak ground acceleration (PGA) and peak ground velocity (PGV) in three mutually perpendicular directions for the three strong earthquakes are given. By comparison the spatial distribution fields of PGA and PGV due to the three strong earthquakes with the distributions of the landslide points, the possible correlations between them are qualitatively analyzed. For strike slip earthquakes, such as the Jiuzhaigou earthquake, the comparisons of distributions of the landslide points with the components of ground motion parameters in three directions indicate that distributions of landslide points relate well to PGA and PGV in horizontal directions including the parallel and normal to the fault strike. Generally, the length of landslide distributions along the fault strike is less than the strike length of the fault for strike earthquakes. Therefore, the slip modes of the strike earthquakes significantly affect the distributions of landslides. For the reverse slip earthquakes, such as the Wenchuan or Lushan earthquakes, distributions of the landslide points relate to ground motion components in all directions, which makes more slide points in reverse earthquakes than those in strike events. Moreover, distributions of the landslides in the near fields of earthquakes are significantly affected by the focus parameters including the slip angle of rupture motion, focus mechanisms and fault scales. Although the case for normal events not shown, the present research indiacte that the further research on the effect of ground motions from normal slip events on landslide distributions is needed.

Keywords: Lushan earthquake; Wenchuan earthquake; Jiuzhaigou earthquake; Landslide; Ground motions

1. Introduction

The correlations between the earthquake induced landslides and the earthquake intensity parameters have been noted by many authors (Tian et al., 2019; Xu et al., 2018, 2010, 2015a, 2015b, 2013; Dai et al., 2011; Meunier et al., 2007; Oglesby et al., 2000, 2001, 2002). For the researches on the correlations between earthquake induced landslides and strong ground motions, most works focus on the earthquake intensity parameters of peak ground acceleration (PGA) and peak ground velocity (PGV). In these works, the parameters of PGA and PGV are calculated by empirical ground motion attenuation relations. The empirical ground motion attenuation relations which exclude the earthquake focus parameters are statistical results (Abrahamson et al., 2014; Boore et al., 2014), so their descriptions for the variation of earthquake ground motion sometimes neglect the fault geometry parameters or rupture motion. Although, some of empirical ground motion attenuation relations have less biases in the near fields of earthquakes (Bai, 2017). Variations of PGA and PGV, especially in the near field of the epicenter or earthquake fault, are significantly affected by the earthquake fault scales and details of the fault rupture dynamics (Ma and Liu, 2006) and then cast the effects on the earthquake induced landslides. Although there are some researches on the effect of the ground motion characters on the earthquake induced landslides, such as Song et al (2018), the researches on the correlations between the near field ground motion fields and landslide distributions are not many at present. In general, the strong ground motion stations in the near field of earthquake source are scarcity. Therefore, the efficient way to describe variations of ground motions in the near field of earthquakes is to construct the ground motion fields by theoretical simulations.

There are many methods to reconstruct strong ground motions due to earthquakes. At the beginning of strong ground motion simulations, the finite-element (Ma and Liu, 2006) and finite-difference (Vidale et al., 1988) methods are often used. Later, it is found that these methods have some disadvantages, such as the larger cost of computation and the frequency band limited to the low scope. After the analyses of the correlations between the seismic parameters of earthquake fault rupture (Schmedes et al., 2010; Olsen et al., 2009; Mai and Beroza, 2002; Oglesby and Day, 2002) and those of ground motions, the stochastic methods of ground motion simulations were then put forward. Using the stochastic methods of ground motion simulations can overcome the weakness of the finite-element and finite-difference methods. Computed a large number of dynamic strike and dipping fault rupture models by the finite-element method, Schmedes et al (2010) constructed a kinematic rupture model that incorporated the key characteristics extracted from the dynamic rupture models. Meanwhile, they validated the rupture model using observed strong motion recordings of the near field for the 1994 Northridge earthquake and the 1989 Loma Prieta earthquakes. Overall, the new rupture model of Schmedes et al (2010) yielded a better prediction for the two validation events. Computing the synthetic broadband seismograms by using the method of Liu et al (2006), they also performed comparisons with the rupture model of Liu et al (2006). Then, Schmedes et al (2010) proposed a new rupture model generator based on their research achievements. The new model can be used in predicting observed PGA and PGV in the broadband frequencies (0 - 10 Hz). Therefore, the rupture model generator of Schmedes et al (2010) is applied to reconstruct the near field ground motion in this work.

In the past twenty years, there are many earthquake induced landslides happened in Sichuan province, China. These landslides are induced by the Wenchuan, Lushan, and Jiuzhaigou earthquakes. There are at least 190,000, 15,000 and 5,900 earthquake induced landslide points (Tian et al., 2019; Xu et al., 2018; 2015a; 2015b; 2013; 2010; Dai et al., 2011) during the Wenchuan, Lushan, and Jiuzhaigou main shocks. According to the recent study on the potential source area of Sichuan province, the Longmengshan and Huya faults have relative higher upper-limit of earthquake magnitude. Meanwhile, the magnitudes of the Wenchuan, Lushan and Jiuzhaigou earthquakes are very close to the upper-limit of earthquake magnitudes of their corresponding potential source areas. Moreover, there are many landslides happened in the region near these earthquake epicenters. Therefore, the Wenchuan, Lushan and Jiuzhaigou earthquakes are firstly selected to reconstruct the ground motion fields in this work. During the computing, the broadband simulation of strong ground motion method of Schmedes et al (2010) is used. Then the simulation results are validated by the proceeding research achievements on the slip distributions of the three earthquake faults and

the strong motion recording data. Meanwhile, the contours of PGA and PGV caused by these earthquakes are attained. At last, the correlations between the distributions of ground motion parameters (PGA and PGV) and the landslide positions are qualitatively analyzed.

2 Three Earthquakes and the Corresponding Parameters

The Jiuzhaigou earthquakes occurred on 8 August 2017 is the strike slip event. The M_s (surface magnitude) of this earthquake is 7.0. The epicenter of Jiuzhaigou earthquake is 103.82°E and 33.20 °N (Zheng et al., 2017). The Wenchuan and Lushan earthquakes are the reverse rupture motion. The M_s of these two earthquakes are 8.0 and 7.0. The epicenter of the Wenchuan earthquake is 103.40°E and 31.00°N (Meng et al., 2011). Differing from the Wenchuan earthquakes, the Lushan earthquake is blind reverse event (Xu et al., 2013). The epicenter of the Lushan earthquake is 103.00°E and 30.30°N (Xu et al., 2013). Compared with the Lushan and Jiuzhaigou earthquakes, the fault size of the Wenchuan earthquake is much larger and the landslide points more. There are three segments of the Longmenshan fault belt contributed to the rupture motion of the Wenchuan earthquake (Wang et al., 2008). Due to the computational limit of the kinematic rupture model generator (Schmedes et al., 2010), we choose the middle and south segment of the central part of the Longmenshan faults, which is the biggest one of the three segments, as the simulation fault. During the reconstruction of the ground motions of three earthquakes, the main shocks are only considered. The last used fault parameters of the three earthquakes are referred to Wang et al (2008, 2013) and Zheng et al (2017) and listed in Table 1. In order to compute the wave fields caused by the three earthquakes, the layer models in the regions should be given. Therefore, the crustal model of Michael Bevis (2017) is used. As shown in Figure 1, three regions that cover the three earthquake faults are selected to reconstruct the ground motion fields. In Figure 1, region I contains region II. Therefore we only calculate the layer model for region I. For the region I, at least four control points is selected and their crustal layer parameters are obtained by the crustal model (Michael Bevis, 2017). Lastly, the mean layer model of regions of I and II are approximated by the mean values of crustal parameters at the control points. Following the same procedure, the mean layer model of region III is obtained. As the summary, the mean layer models of regions I, II, and III are listed in Table 2 and 3. After the layer parameters (such as density, shear and elastic modulus) achieved, the quality factor for S- and P-wave are computed following the method of Mavko (2005) and Wang et al (2009).

3 Computation Method and Model

By analyzing 315 dynamic rupture models of the world computed up to 5.0 Hz, Schmedes et al (2010) quantitatively described the correlations and amplitude distributions of earthquake source parameters, such as slip, rise time. Then, a database contains the epistemic uncertainty of the problem is constructed. Based on this database, the probability density functions for the amplitude distributions of the source parameters and their correlations are calculated. Applying these amplitude distributions and correlations of the source parameters, the slip distribution on the fault during the happening of earthquakes are constructed. Lastly, combing the slip distributions on the fault and regional Green's function results (Aki and Richards, 1980), the ground motion at a given site can be calculated. Here, the regional Green's function is computed by the method of Herrmann (1978; 1979) and Wang and Herrmann (1980). The advantage of the method of Herrmann et al (1978; 1979) is that the three dimensional layer medium can by simplified to the two dimensional case and then the Green's function can be computed efficiently in the cylinder coordinates. Therefore, based on the layer parameters in Table 2 and 3 and the regional Green's function computation method, the Green's function results for the target regions I, II, and III (in Fig 1) can be achieved. After the slip distribution on the earthquake fault and the regional Green's function computed, the distributions of strong ground motions in the near field of the earthquake are computed following the method of Spudich (1980).

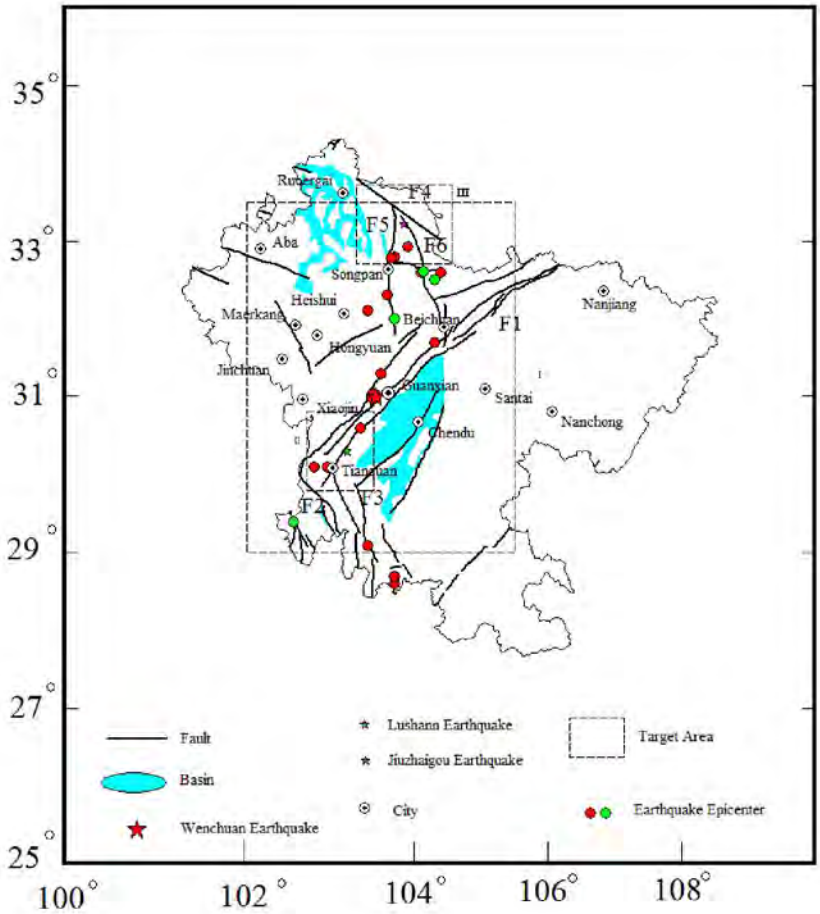

Fig. 1 - The research area and the epicenters of earthquakes

F1- Longmenshan fault; F2-Xianshuihe fault; F3-Yingjing-Mabian fault; F4-Tazang fault;

F5- Minjiang fault; F6-Huya fault; The dash boxes corresponding to the target areas of I, II, and III

Table 1 –The fault parameters of the three earthquakes

Parameters	**Fault Length**(km)	**Fault Dip angle** (°)	**Fault Dip Width** (km)	**Strike Direction** (°)	**Slip Angle** (°)	**Seismic Momen** (N●m)	**Moment Magnitude**
Wenchuan	200	60	23	229	118	1.04×10^{21}	7.9
Lushan	60	38	30	205	96	1.54×10^{19}	6.7
Jiuzhaigou	46	85	26	151	-4	6.9×10^{18}	6.5

Table 2 – The mean lay parameters of target are I and II

Lay number	P-wave velocity (km/s)	S-wave velocity (km/s)	Density (kg/m^3)	Thick (km)	Elastic Modulus (GPa)	Shear Modulus (GPa)
1	3.1	1.5	2.9	2.9	17.7	6.8
2	6.1	3.5	2.7	18.1	85.5	34.3
3	6.4	3.69	2.8	17.4	95.2	37.9
4	6.9	3.96	2.94	10.5	115.9	46.0

Table 3 − The mean lay parameters of target are III

Lay number	P-wave velocity (km/s)	S-wave velocity (km/s)	Density (kg/m^3)	Thick (km)	Elastic Modulus (GPa)	Shear Modulus (GPa)
1	6.1	3.5	2740	22.4	85.9	34.5
2	6.3	3.6	2780	19.9	92.3	37.0
3	7.0	3.9	2950	8.6	118.2	46.9

4. Validations of the Simulation Results

The fault slip distributions for the three earthquakes are firstly calculated based on the kinematic rupture model generator of Schmedes et al (2010). The fault slip distributions of the Wenchuan, Lushan and Jiuzhaigou earthquakes are shown in Figure 2 to 4. As indicated by these figures, the maximum of slip and the slip distribution are almost approximated to the inversion of fault slips by telescope seismic data (Wang et al., 2008, 2013; Zheng et al., 2017), especially for the distributions of the Lushan and Jiuzhaigou earthquake fault slip. Because the earthquakes with Mw ≥ 7.9 are fewer in the databank of Schmedes et al (2010), the fault slip distribution of the Wenchuan earthquake computed here is little different from that of inversion achievements. However the maximum slip and its location are approximated to the existing achievements on the Wenchuan earthquake fault slips. Therefore, the simulation of ground motion that is based on the fault slip is reasonable for the computation of ground motions of the three earthquakes.

In the near field of the Jiuzhaigou earthquake, the strong motion stations are scarcity. Because the Wenchuan earthquake is more complex and contributed by the rupture motions of the three segments of faults (Wang et al, 2008), the approximated fault model are selected here. Therefore, we do not use the recordings of the Wenchuan earthquake to compare with the computational results. To valid the computation results at the ground surface, the recordings of station of 51YAM (103.10°E, 30.10°N) with the distance to the Lushan earthquake epicenter being 24 km are lastly selected to compare with the simulation results. Figure 5 plots the acceleration time histories of the 51YAM station recordings and the simulation result at the location of the 51YAM station for the Lushan earthquake. The recording time histories for the north-south (NS) and east-west (EW) components at the station of 51YAM are not transformed to the components parallel and normal to the Lushan fault. However, ground acceleration time histories of the simulations at the station of 51YAM are approximated to those of real recordings. Hence, the broadband method of Schmedes et al (2010) to simulate the ground motion due to the three earthquakes is reasonable.

5. Results and Discussion

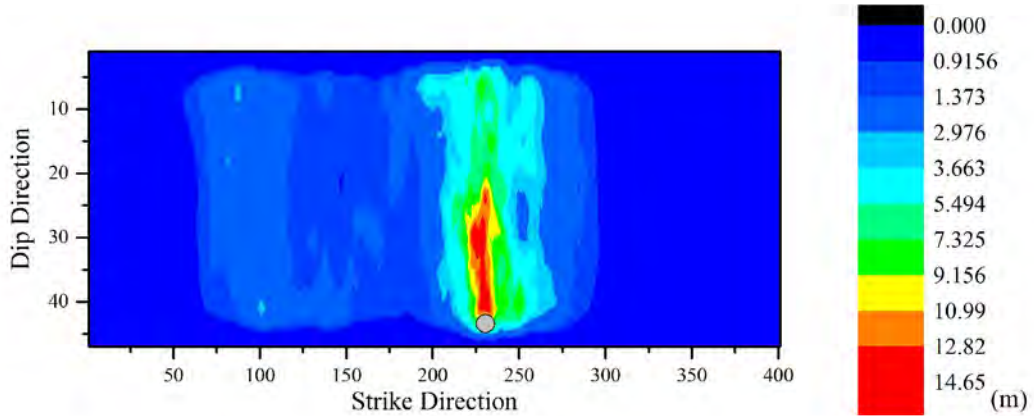

Fig. 2 - The slip distribution on the Wenchuan earthquake fault.

The gray circle is the location of the earthquake focus

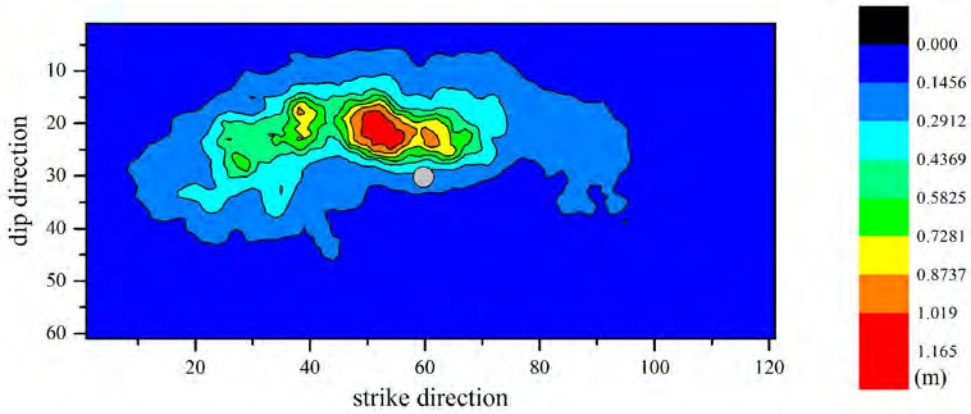

Fig.3 - The slip distribution on the Lushan earthquake fault.

The gray circle is the location of the earthquake focus.

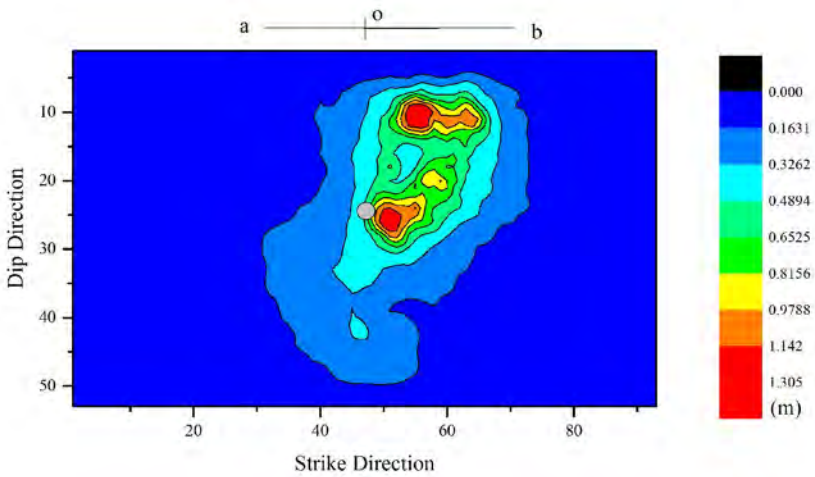

Figure 4 The slip distribution on the Jiuzhaigou earthquake fault.

The gray circle is the location of the earthquake focus. The line ab is the fault slip scope along the strike.

The dot of o is the surface projection of the hypocenter.

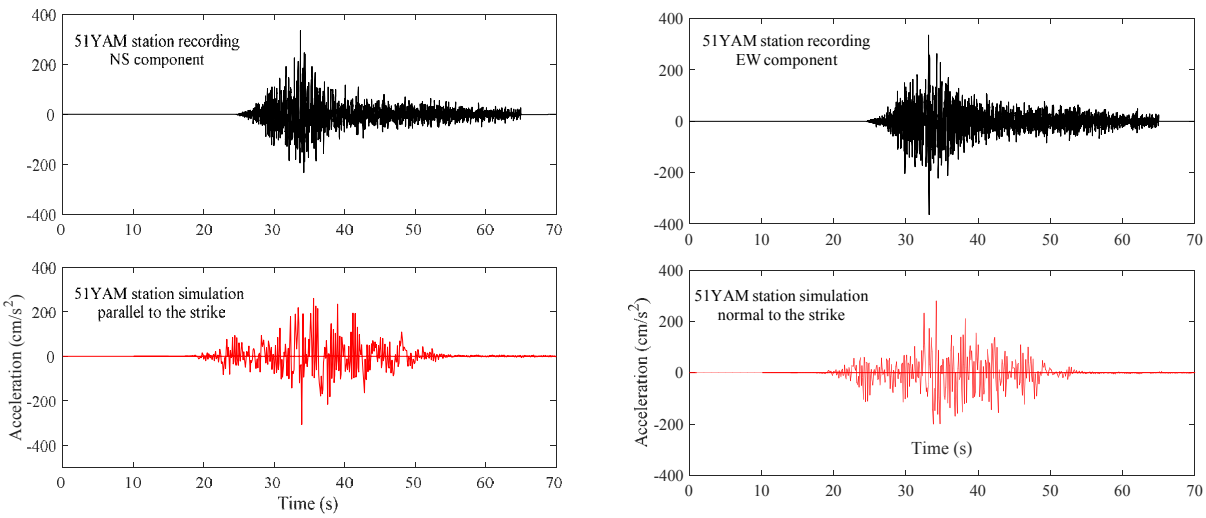

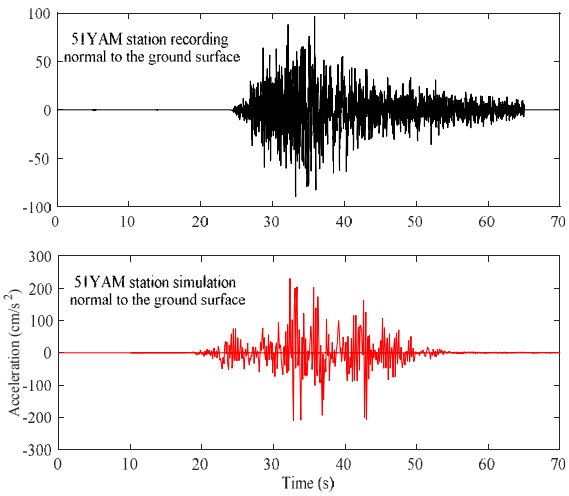

Fig. 5 - Comparison of the acceleration time histories of the 51YAM station recording and the simulation results at the location of the 51YAM station. The black lines are the 51YAM station recordings. The red lines are the computation result of the broadband simulation at the location of the 51YAM station.

Figure 6 is the contours of PGA and PGV in parallel and normal to Wenchuan fault strike direction. Meanwhile, PGA and PGV components normal to the ground surface are also shown. The shapes of the PGA and PGV contours of the Wenchuan earthquake approximate to those achieved by station recordings (Wang et al., 2010). As shown by Figure 6, the correlations between the horizontal PGA and the landslide point distributions are relatively better. Besides the landslide distributed in the scope of the Wenchuan earthquake fault surface projection, there are many landslides distributed outside of the scope the fault scale, especially in the northeast part of region I (Fig. 1). Because the slip angle of the rupture motion of the Wenchuan earthquake fault is 118°(Table 1; Wang et al., 2008) and the hypocenter located at the southwest part of the fault, most landslide points in the northeast part of region I are possibly related to the strike rupture motion of the Wenchuan earthquake. The local slip velocity of the points on the fault (Oglesby and Day, 2002) generally increases with the distance to hypocenter (Schmedes et al., 2010), so the relatively higher slip velocity in the northeast part of the Wenchuan earthquake fault perhaps results into the significant directivity effect in northeast direction. As a result of this, there are many landslide points distributed in the northeast of region I where are outside of the surface projection of the Wenchuan fault.

Figure 7 plots the PGA and PGV contours in parallel and normal to Lushan fault strike direction. At the same time, PGA and PGV components normal to the ground surface are shown. According to the achievements of Xu et al (2015a, b), the Lushan earthquake induced landslides are mainly distributed in the regions with PGA ≥ 200 gal. As indicated by Figure 7 (a)-(c), most of the landslide points distribute in regions with PGA larger than 200 gal in all directions. Therefore, the simulated PGA in Figure 7 is

reasonable. Moreover, from Figure 7, the density of landslide points is much larger in the region with larger PGA. For the PGV normal to the strike, as shown in Figure 7 (e), the larger density of landslide distribution points does not correlate well with the values of PGV. The PGA components in parallel and normal to the fault strike direction relate better to the distribution of landslide points. For the parameter of PGV, the components in direction parallel to fault strike direction relate well to the landslide point distributions. Compared with the parameter of PGV, PGA relates better to the landslide point distributions. The slip angle of the Lushan earthquake (96°, see Table 1) is smaller than that of the Wenchuan earthquake. Meanwhile, the size of the Lushan earthquake fault is much smaller than that of the Wenchuan events. In general, when the fault length is less some threshold, the earthquake directivity effect usually increases with the fault length (Schmedes et al., 2008). Hence, the directivity effect in the strike direction for the Lushan earthquake is not significant. As a result, there are relatively fewer landslide distributed outside of the northeast of the fault surface projection. Similar with the Wenchuan earthquake, most of the landslide points are located at the hanging wall of the Lushan earthquake fault, which results from the fact that the intensity of ground motions in all directions are much stronger at the hanging wall of the fault than those at the foot wall.

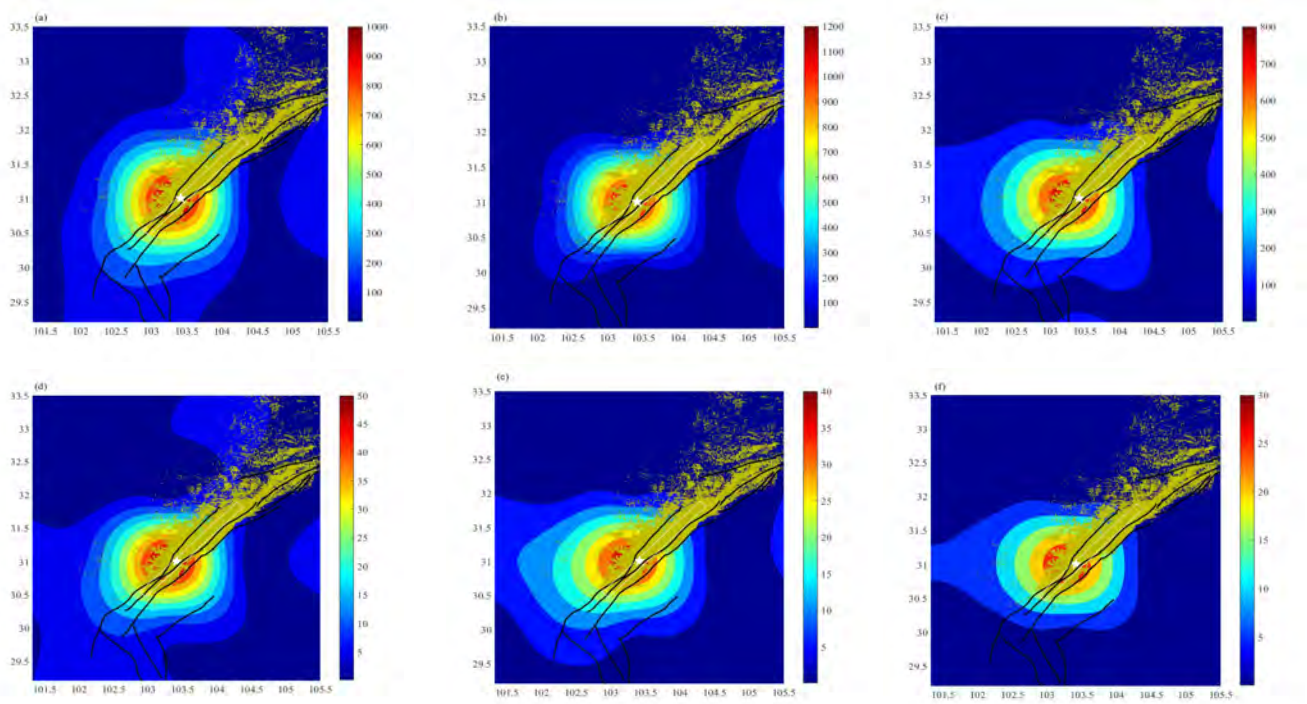

Fig. 6 - The distributions of ground motions and landslides for the Wenchuan earthquake.

(a)-(c) is PGA components in parallel and normal to fault strike and vertical to the ground surface directions. (d)-(f) is PGV components in parallel and normal to fault strike and vertical to the ground surface directions. Little green dots are the landslide points. White star is the epicenter of the Wenchuan earthquake. The rectangle is the fault surface projection.

Figure 8 illustrates the contours of PGA and PGV in parallel and normal to Jiuzhaigou fault strike direction. At the same time, PGA and PGV components normal to the ground surface are given. As indicated by Figure 8, the landslide points are mainly distributed in the region with PGA ≥ 300 gal and PGV ≥ 15 cm/s. Because the dip direction of the Jiuzhaigou earthquake fault is southwest (An et al., 2018; Xu et al., 2018) and the motion of the fault sinistral slip (slip angle is -4°, Table 1), the landslide points distributed on the footwall of the fault are relatively fewer. Furthermore, the dip angle of the Jiuzhaigou fault is 85° (Table 1), so the effect of uplift motion of the fault on the landslide points are not significant. Therefore, the

landslide points are mainly caused by the horizontal movement of the Jiuzhaigou earthquake ground motion. Differing from the Wenchuan and Lushan earthquakes, Figure 8 shows that the landslide points of the Jiuzhaigou earthquake do not fill the area of the fault surface projection, especially in the two ends of the fault. Hence, the length of the Jiuzhaigou fault in the strike direction applied by the focus inversion researches (Zheng et al., 2017) and this work is larger than that of landslide distribution in the strike direction. However, the length of landslide point distribution along the strike of the Jiuzhaigou earthquake fault is almost equal to that of the fault slip region whose slip is larger than background slip of the fault, as indicated by the line of ab in Figure 4. Accordingly, the slip modes of the fault caused by the strike earthquake events probably decide scopes of the landslide point distributions along the fault strike direction.

Because the dip angles of the strike events (such as the Jiuzhaigou earthquake) are generally steeper than those of reverse ones, the uplift motion of the hanging wall due to the extrusion motion between two walls of the fault is less significant. Therefore, the landslide points caused by the strike slip events are mainly related to the horizontal components of ground motions. In the near field of the strike events, the maximum distribution scopes of the landslide points along the strike direction are mainly decided by the slip mode of the fault. However, the uplift motions of the hanging walls for the reverse earthquake events are significant, as called the hanging wall effect now. Therefore, besides the horizontal components of ground motions, the landslide points caused by the reverse events are also related to ground motion components vertical to the ground surface. In the near field of the reverse events, the landslide points mainly distribute in the surface projection of the earthquake fault. Moreover, because of the significance of the uplift motion of the hanging wall, there are more landslide points distributed at the hanging wall of the reverse events than those at the footwall. For the large sizes of earthquake faults, such as the Wenchuan earthquake fault, the directivity effects of ground motion are important factors causing landslides. Because the normal slip earthquakes and their induced landslides are scarcity in China, the comparisons of the ground motion contours and landslide point distributions are not shown. However, these are important issues for the future work. The above analyses give some insights of the correlations between the fault rupture motion and landslide distributions. Hence, the present work is helpful to the researches on the inferences of earthquake focus parameters through landslide spatial distributions.

6. Conclusions

By the qualitatively analyses on the correlations between PGA and PGV in the near field of the three large earthquakes and spatial distributions of landslide points, main conclusions are: (1) distributions of earthquake induced landslides related to the horizontal ground motion components, especially for the cases of strike slip earthquakes. (2) because of dip angles of reversal slip earthquakes being generally gentle and uplift motions of hanging wall significant, more earthquake induced landslides distribute on the hanging wall or in the surface projection of the fault. (3) because of the local slip velocities of points on the fault tend to accelerate with the increasing distance to the focus, larger scales of earthquake faults, such as the Wenchuan earthquake, probably have larger local slip velocity for the points of the fault far away from the focus. As results of this, there are many earthquake induced landslides distribute out of the fault surface projection along the larger scale direction of the fault. (4) for the strike slip earthquakes, the maximum distribution scope of earthquake induced landslide along the strike of the fault is probably less than the strike size of the real earthquake fault and affected by the slip mode of the fault rupture.

7. Acknowledgements

The Basic Research Project of Institute of Geology, China Earthquake Administration (IGCEA1909) and the Active Fault Survey Project for Aba Prefecture, Sichuan, China (IGCEA-X1906G) supported this work. Meanwhile, we thank Dr, Schmedes for his discussion on the broadband simulation of strong ground

motions. We also thank the China Strong Motion Network Center at Institute of Engineering Mechanics, China Earthquake Administration for providing us the strong motion recording data for the Luhan earthquake.

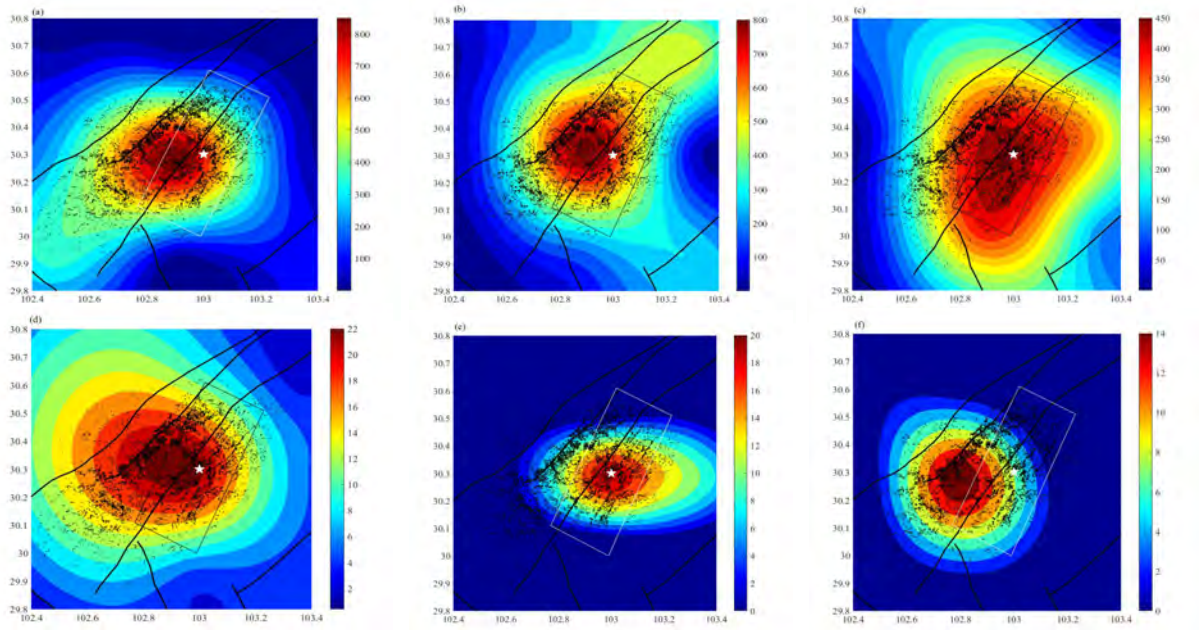

Fig. 7 - The distributions of ground motions and landslides for the Lushan earthquake.

(a)-(c) is PGA components in parallel and normal to fault strike and vertical to the ground surface. (d)-(f) is PGV components in parallel and normal to fault strike and vertical to the ground surface. Little black dots are the landslide points. White star is the epicenter of the Lushan earthquake. The rectangle is the fault surface projection.

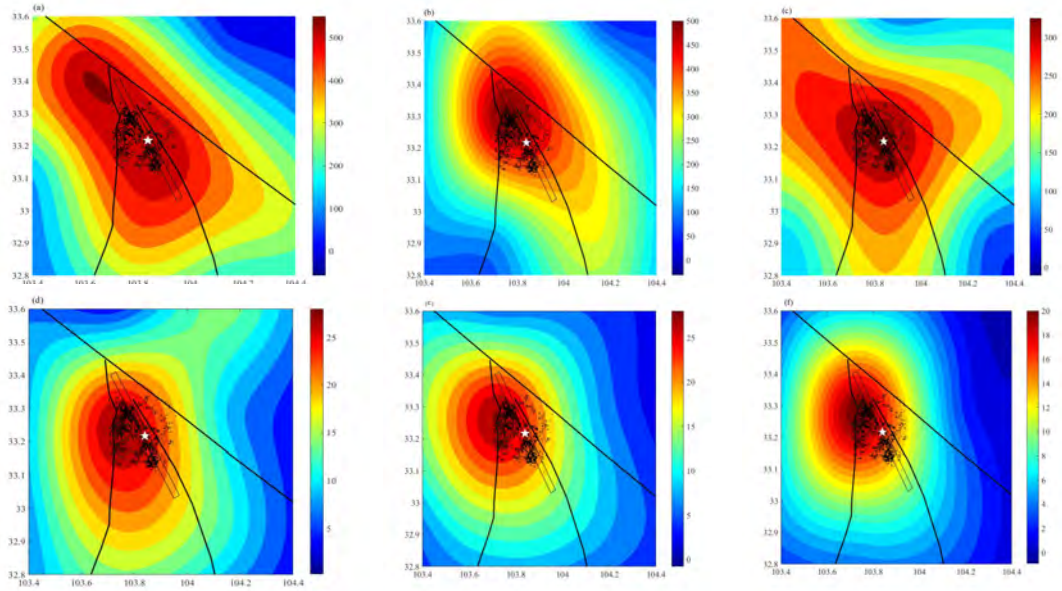

Fig. 8 - The distributions of ground motions and landslides for the Jiuzhaigou earthquake.

(a)-(c) is PGA components in parallel and normal fault strike and vertical to the ground surface. (d)-(f) are PGV components in parallel and normal fault strike and vertical to the ground surface. Little black dots are the landslide points. White star is the epicenter of the Jiuzhaigou earthquake. The rectangle is the fault surface projection.

8. References

[1] Aki K, Richards P G (1980): Quantitative seismology: theory and methods. Freeman, San Francisco, California.

[2] Abrahamson NA, Silva W J, Kamai R (2014): Summary of the ASK14 ground motion relation for active crustal regions. *Earthquake Spectra*, **30** (3), 1025-1055.

[3] An Y R, Su J R, Xue Y, et al (2018): Seismologic characteristics of the 2017, M 7.0 Jiuzhaigou, Sichuan, earthquake. *Chinese Science Bulletin*, **63** (7), 663-673.

[4] Bai Y Z (2017): Comparison of strong ground motion recordings of the Lushan, China, earthquake 20 April 2013 with the Next Generation Attenuation (NGA) - West2 ground-motion models. *Bulletin of the Seismological Society of America*, **107** (4), 1724-1736.

[5] Boore D M, Stewart J P, Seyhan E, et al (2014). NGA-West2 equations for predicting PGA, PGV, and 5% damped PSA for shallow crustal earthquake. *Earthquake spectra*, **30** (3), 1057-1085.

[6] Dai F C, Xu C, Yao X, et al (2011): Spatial distribution of landslides triggered by the 2008 Ms 8.0 Wenchuan earthquake, China. *Journal of Asian Earth Sciences*, **40** (3), 883-895.

[7] Herrmann R B (1978): A note on causality problems in the numerical synthesis of elastic wave propagation in cylindrical coordinate system. *Bulletin of the Seismological Society of America*, **68** (1), 117-123.

[8] Herrmann R B (1979): SH wave generation by dislocation sources- A numerical study. *Bulletin of the Seismological Society of America*, **68** (1), 1-16.

[9] Liu P, Archuleta R J, Hartzell S H (2006): Prediction of broadband ground-motion time histories: Hybrid low/high-frequency method with correlated random source parameters. *Bulletin of the Seismological Society of America*, **96** (6), 2118-2130.

[10] Ma S, Liu PC (2006): Modeling of the perfectly matched layer absorbing boundaries and intrinsic attenuation in explicit finite-element methods. *Bulletin of the Seismological Society of America*, **96** (5), 1779-1794.

[11] Mai PM, Beroza GC (2002): A spatial random field model to characterize complexity in earthquake slip. *Journal of Geophysics Reserach*, **107** (B11), 10.1029/2001jb000588.

[12] Mavko G (2005): A theoretical estimation of S-wave attenuation in sediment. SEG/Houston Annual Meetion, 2005.

[13] Meng LY, Shi BP (2011): Near-fault strong ground motion simulation of the May 12, 2008, M_w 7.9 Wenchuan earthquake by dynamical composite source model. *Chinese Journal of Geophysics*, **54** (4), 1010-1027 (in Chinese with English Abstract).

[14] Meunier P, Hovius N, Haines AJ (2007): Regional patterns of earthquake-triggered landlides and their relation to ground motion. *Geophysical Researche Letters*, **34**, L20408, doi: 10.1029/2007GL031337.

[15] Michael B. The Crust 1.0 model. https://igppweb.ucsd.edu/~gabi/crust1.html.

[16] Oglesby DD, Archuleta RJ, Nielsen ST (2000): The three-dimensional dynamics of dipping faults. *Bulletin of the Seismological Society of America*, **90** (3): 616-628.

[17] Oglesby DD, Day SM (2001): Fault geometry and the dynamics of the 1999 Chi-Chi (Taiwan) earthquake. *Bulletin of the Seismological Society of America,* **91**(5), 1099-1111.

[18] Oglesby DD, Day SM (2002): Stochastic fault stress: Implications for fault dynamics and ground motion. *Bulletin of the Seismological Society of America*, **92** (8), 3006-3021.

[19] Olsen KB, Day SM, Dalguer LA, et al (2009): ShakeOut-D: Ground motion estimates using an ensemble of large earthquakes on the southern San Andreas fault with spotaneous rupture propagation. *Geophysical Research Letter*, **36** (4), L0403, 10.1029/2008GL036832.
[20] Schmedes J, Archuleta RJ (2008): Near-source ground motion along strike slip faults: Insights into magnitude saturation of PGV and PGA. *Bulletin of the Seismological Society of America*, **98** (5), 2278-2290.
[21] Schmedes J, Archuleta RJ, Lavallee D (2010): Correlation of earthquake source parameters inferred from dynamic rupture simulations. *Journal of Geophysical Research*, **115** (B3), B03304, doi: 10.1029/2009JB006689.
[22] Song J, Gao YF, Feng TG (2018): Probabilistic assessment of earthquake-induced landslide hazard including the effects of ground motion directionality. *Soil Dynamics and Earthquake Engineering*, **105**, 83-102.
[23] Spudich P (1980): The Dehoop-Kinopoff representation theorm as a linar inverse problem, *Geophysical Research Letter*, 7(9), 717-720.
[26] Tian Y, Xu C, Ma S, et al (2019): Inventory and spatial distribution of landslides triggered by the 8 August 2017 Mw 6.5 Jiuzhaigou earthquake, China. *Journal of Earth Science*, **30** (1), 206-217.
[27] Vidale JE, Helmberger V (1988): Elastic finite-difference modeling of the 1971 San Fernando, California earthquake. *Bulletin of the Seismological Society of America*, **78** (1), 122-141.
[28] Wang CY, Herrmann RB (1980): A numerical study of P, SV and SH wave generation in a plane layered medium. *Bulletin of the Seismological Society of America*, **70** (4): 1015-1036.
[29] Wang D, Xie LL, Abrahamson NA (2010): Comparision of strong ground motion from the Wenchuan, China, earthquake of 12 May 2008 with the Next Generation Attenuation (NGA) ground-motion models. *Bulletin of the Seismological Society of America* **100** (5B), 2381-2395.
[30] Wang WM, Zhao LF, Li J, et al (2008): Rupture process of the M_s 8.0 Wenchuan earthquake of Sichuan, China. *Chinese Journal of Geophysics*, **51** (5): 1403-1410 (in Chinese with English Abstract).
[31] Wang WM, Hao JL, Yao ZX (2013): Preliminary result for rupture process of Apr. 20, 2013, Lushan earthquake, Sichuan, China. *Chinese Journal of Geophysics*, **56** (4), 1412-1417 (in Chinese with English Abstract).
[32] Wang Y, Liu J, Shi Y, et al (2009): PS-wave Q estimation based on the P-wave Q values. *Journal of Geophysics and Engineering*, **6** (4), 386-389.
[33] Xu C, Dai FC, Xu XW (2010): Wenchuan earthquake-induced langdslides: an overiew. *Geological Review*, **56** (6), 860-874 (in Chinese with English Abstract).
[34] Xu C, Xu XW, Zheng WJ, et al (2013): Landslides triggered by the April 20, 2013 Lushan, Sichuan province Ms 7.0 strong earthquake of China. *Seismology and Geology*, **35** (3), 634-660 (in Chinese with English Abstract).
[35] Xu C, Xu XW, Bruce J, et al (2015a): Database and spatial distribution of landslides triggered by the Lushan, China, Mw 6.6 earthquake of 20 April 2013. *Geomorphology*, **248**, 77-92.
[36] Xu C, Xu XW, Bruce J, et al (2015b): Landslides triggered by the 20 April 2013 Lushan, China, Mw 6.6 earthquake from field investigations and preliminary analyses. *Landslides*, **12** (2), 365-385.
[37] Xu C, Wang SY, Xu XW, et al (2018): A panorama of landslides triggered by the 8 Auguse 2017 Jiuzhaigou, Sichuan Ms 7.0 earthquake. *Seismology and Geology*, **40** (1), 232-260 (in Chinese with English Abstract).
[38] Zheng XJ, Zhang Y, Wang RJ (2017): Estimation the rupture process of the 8 August 2017 Jiuzhaigou earthquake by inverting strong motion data with IDS method. *Chinese Journal of Geophysics*, **60** (11), 4421-4430 (in Chinese with English Abstract).

